Super-Twisting Sliding Mode Control with Adaptive Gain of Quadrotor with Rigid Manipulator

Hardy Bin Anuar, Franck Plestan, Abdelhamid Chriette, Olivier Kermorgant

Super-Twisting Sliding Mode Control with Adaptive Gain of Quadrotor with Rigid Manipulator

Hardy Azmir Bin Anuar, Franck Plestan, Abdelhamid Chriette and Olivier Kermorgant

***Abstract*— This paper presents the control of an aerial manipulator composed of a quadrotor and a manipulator with two degrees of freedom (2 DOF). There is a strong physical coupling between the dynamics of the UAV and the manipulator arm. This coupling along with external perturbations (e.g. wind gusts), considerably affects the stability of the drone's motion in flight which, consequently, affects the desired accuracy of the end effector with respect to its final task. The solution presented here is based on super-twisting sliding mode control with adaptive gain. It is a continuation of previous study on sliding mode control with adaptive gain [1]. The effectiveness of the controller and its robustness against perturbations are verified and analyzed using numerical simulation.**

I. Introduction

UAVs have been a topic of research in many domains, such as military, civilian, academic and industrial applications. For various reasons, most studies tend to focus on quadrotor UAV that has 4 rotors. One of its advantages is that it does not require mechanical linkages to vary the rotor blade pitch angle as compared to scaled helicopter because its motion is controlled by changing the 4 rotors speed. The use of 4 rotors allows each rotor to have smaller diameter, that will reduce the possibility of damaging the rotors if quadrotor hits an object. Quadrotor also requires only a small area for vertical taking-off and landing (VToL). An other advantage is the capability to fly in every direction, vertically and horizontally, to hover in a fixed position and to fly at a low altitude. These abilities make them the perfect instrument for detailed surveillance, remote sensing and flying through hard-to-reach areas.

Due to its advantages, a quadrotor is a suitable UAV for the base of aerial manipulation to perform an active task such as grasping, transporting, positioning, measuring, assembling or disassembling mechanical parts of any objects. To accomplish manipulation task in the air, UAV needs to be equipped with one or several robotic manipulators, hence the name *unmanned aerial manipulator* (UAM) [2]. The application of UAM to access high-location and hard-to-reach areas that involve significant risks and accidents can be very helpful. This aerial manipulator can be remotely controlled, semi-autonomous or autonomous.

The control of the motion of a quadrotor equipped with a manipulator arm is a hard problem, given that, on the one hand, the quadrotor is an under-actuated system with two directions that are not directly actuated, and, on the other hand, the existence of an additional torque caused by the motion of the arm that disturbs the stability and the accuracy of the positioning task of the full system {quadrotor+arm}. Based on the compensation of the coupling between a UAV and a manipulator, Mimmo *et al* [3] proposed a control scheme that is able to let the end-effector to track a desired reference while the UAV is maintained at a constant position. The manipulator is stabilised by compensating the UAV attitude whereas the joint torque is use in the computation of UAV control law. The interconnection of these two subsystems has been proven to be stable.

Kim *et al* [4] developed an adaptive sliding mode controller (SMC) with estimated uncertainty to cope with this disturbance. An experimental demonstrates satisfactory performance for picking up and delivering an object. As the motion of the manipulator may disturb the attitude of UAV that affects the flight stability and the operation accuracy, Zhiyuan *et al* [5] proposed a fuzzy SMC with extended state observer for estimating disturbance. The fuzzy controller reduces the chattering effect of SMC. Chen *et al* [6] discuss tracking control strategy due to internal and external disturbance. These disturbance are handled in two parts: a position controller using a robust SMC and an attitude controller using an adaptive controller with disturbance observer.

Super-twisting sliding mode controller (STWC) is designed to reduce chattering effect significantly compared to standard SMCs. A STWC of a quadrotor-based aerial manipulator is proposed in Kuchwa-Dube *et al* [7] for altitude and attitude tracking with the manipulator in motion. It is shown that the controller provides good altitude and attitude tracking compared to SMC. Overall, STWC has reduced control effort with lower error and reduces the chattering effect significantly. Kuchwa-Dube *et al* [8] also study the performance of adaptive gain super-twisting controller (STWCA) and its modified version compared to standard STWC. The test yield an improved altitude and attitude tracking with the modified version provide the best tracking performance.

In this paper, in terms of dynamic modelling, the approach of considering the dynamic modelling of the UAV independently from that of the manipulator arm is detailed. A model for the full system is built based on the compensation of the coupling effect between UAV and manipulator arm which is considered as an external disturbance.

The main contribution of the paper is on the application STWC scheme with gain adaptation law that is independent of the disturbance bound. As previously studied [1], the controller is applied to UAV simplified model and manipulator

The authors are with Nantes Université, Ecole Centrale Nantes, CNRS, LS2N, UMR 6004, F-44000 Nantes, France. **Corresponding author:** H. Bin Anuar, Hardy.Anuar@ls2n.fr

arm computed torque control. With adaptive gain STWC, it is unnecessary to know the bound of uncertainties; therefore the gain will not be overestimated as with adaptive gain SMC. It is feasible with the proposed scheme to achieve system stability, accuracy and robustness.

II. SYSTEM MODELLING

Deriving UAM dynamic equations requires the definition of reference frames. The inertial frame, also referred as world frame, is denoted F_W and is defined by its origin O_W and three unit vectors along the main axes denoted $\{x_W, y_W, z_W\}$. The compact notation for this definition yields F_W:$O_W - \{x_W, y_W, z_W\}$. The body frame of the multi-rotor is F_B:$O_B - \{x_B, y_B, z_B\}$, where O_B is located at the center of mass (CoM) of the UAV. F_0:$O_0 - \{x_0, y_0, z_0\}$ is the base frame of manipulator attached to CoM of UAV body frame, while F_1:$O_1 - \{x_1, y_1, z_1\}$, F_2:$O_2 - \{x_2, y_2, z_2\}$ and F_e:$O_e - \{x_e, y_e, z_e\}$ are the frames of manipulator link-1, link-2 and end-effector (see Figure 1 for illustration).

A. Multi-rotor UAV Dynamics

The position of O_B expressed in F_W is denoted by $\boldsymbol{\xi} = [x \;\; y \;\; z]^T$. The orientation of the UAV is defined by the three Euler angles of roll, pitch and yaw given by $\boldsymbol{\eta} = [\phi \; \theta \; \psi]^T$. UAV dynamic model is derived from Newton Euler formulation under the following assumptions [9]:

- The structure is rigid and symmetrical.
- The centre of gravity coincide with body fixed frame.
- The propellers are rigid.
- Thrust and drag are proportional to the square of propellers speed.

By applying Newton-Euler equation [10], the simplified nonlinear model for UAV according to [11] and [12] is given by:

$$\ddot{x} = \frac{U_1}{m}(C\psi S\theta C\phi + S\psi S\phi) \tag{1}$$

$$\ddot{y} = \frac{U_1}{m}(S\psi S\theta C\phi - C\psi S\phi) \tag{2}$$

$$\ddot{z} = \frac{U_1}{m} C\theta C\phi - g \tag{3}$$

$$\ddot{\phi} = \frac{U_2}{I_{xx}} + \frac{I_{yy} - I_{zz}}{I_{xx}}\dot{\theta}\dot{\psi} \tag{4}$$

$$\ddot{\theta} = \frac{U_3}{I_{yy}} + \frac{I_{zz} - I_{xx}}{I_{yy}}\dot{\phi}\dot{\psi} \tag{5}$$

$$\ddot{\psi} = \frac{U_4}{I_{zz}} + \frac{I_{xx} - I_{yy}}{I_{zz}}\dot{\phi}\dot{\theta} \tag{6}$$

in which m is the mass of the UAV, $Sx = sin(x)$ and $Cx = cos(x)$ while the control inputs U_1, U_2, U_3 and U_4 are the upward thrust, rolling torque, pitching torque and yawing torque respectively. I_{xx}, I_{yy} and I_{zz} correspond to UAV moment of inertia about x_B, y_B and z_B axis respectively and $g = 9.81\, ms^{-2}$ is the gravitational acceleration.

B. Modelling of Manipulator

The manipulator dynamics are established by the recursive Newton Euler (RNE) algorithm which describes dynamic systems in terms of force and momentum. The RNE algorithm as in [13] consists of two recursive computations: *forward recursive* and *backward recursive*. Detailed discussion of this algorithm can be found in [13] and [14]. If RNE algorithm is symbolically executed, it will form an expression of manipulator dynamic as

$$\boldsymbol{\Gamma} = \boldsymbol{M(q)}\ddot{\boldsymbol{q}} + \boldsymbol{C(q,\dot{q})}\dot{\boldsymbol{q}} + \boldsymbol{Q(q)} \tag{7}$$

where $\boldsymbol{\Gamma}$ is the joint torque vector, $\boldsymbol{q}$ is the joint positions vector, $\boldsymbol{M(q)}$ is the symmetric and positive definite inertia matrix, $\boldsymbol{C(q,\dot{q})}$ is the vector of Coriolis and centrifugal torques and finally, $\boldsymbol{Q(q)}$ is the vector of gravity torques.

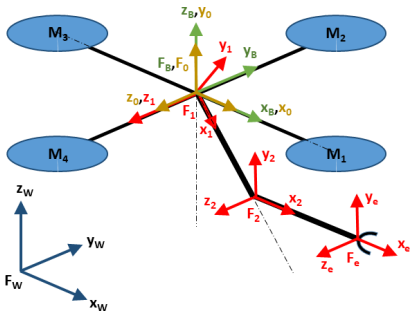

Fig. 1: UAV with a 2-DOF manipulator arm - frames definitions.

C. Modelling of UAM

Modelling of UAM is based on the coupling effect of the manipulator on UAV as external disturbances and vice versa as in [11] and [12]. Manipulator floating base initial velocity ($\boldsymbol{\omega}_0$) and acceleration ($\dot{\boldsymbol{\omega}}_0$, $\dot{\boldsymbol{\nu}}_0$) given by UAV velocity ($\boldsymbol{\omega}$) and acceleration ($\dot{\boldsymbol{\omega}}$, $\ddot{\boldsymbol{\xi}}$) for the RNE algorithm are as follows

$$\dot{\boldsymbol{\nu}}_0 = {}^0\boldsymbol{R}_W(\ddot{\boldsymbol{\xi}} + [0\;0\;-g]^T) \tag{8}$$

$$\boldsymbol{\omega}_0 = {}^0\boldsymbol{R}_B\boldsymbol{\omega} \tag{9}$$

$$\dot{\boldsymbol{\omega}}_0 = {}^0\boldsymbol{R}_B\dot{\boldsymbol{\omega}} \tag{10}$$

where ${}^0\boldsymbol{R}_W$ is the rotation matrix describing the configuration of the manipulator base frame in relation to the world frame and ${}^0\boldsymbol{R}_B$ is a rotation matrix of UAV body frame with respect to manipulator base frame. This velocity and acceleration are transmitted from one link to another and result in an additional resultant torque on joint-j.

The force $\boldsymbol{f}_W$ and torque $\boldsymbol{\tau}_B$ applied to UAV as external disturbance are then obtained from force, $\boldsymbol{f}_0$, and moment, $\boldsymbol{m}_0$, of manipulator base frame and read as

$$\boldsymbol{f}_W = {}^W\boldsymbol{R}_0\,\boldsymbol{f}_0 \tag{11}$$

$$\boldsymbol{\tau}_B = {}^B\boldsymbol{R}_0\,\boldsymbol{m}_0 \tag{12}$$

Eq. (8) to (12) describe the coupling between both the systems (manipulator and UAV) as shown in Fig. 2. As a consequence, from (1) to (6), the update dynamic equations

of UAV for UAM model due to coupling effect read as [11]

$$\ddot{x} = \frac{U_1}{m}(C\psi S\theta C\phi + S\psi S\phi) + \frac{f_{W.x}}{m} \tag{13}$$

$$\ddot{y} = \frac{U_1}{m}(S\psi S\theta C\phi - C\psi S\phi) + \frac{f_{W.y}}{m} \tag{14}$$

$$\ddot{z} = \frac{U_1}{m}C\theta C\phi - g + \frac{f_{W.z}}{m} \tag{15}$$

$$\ddot{\phi} = \frac{U_2 + \tau_{B.\phi}}{I_{xx}} + \frac{I_{yy} - I_{zz}}{I_{xx}}\dot{\theta}\dot{\psi} \tag{16}$$

$$\ddot{\theta} = \frac{U_3 + \tau_{B.\theta}}{I_{yy}} + \frac{I_{zz} - I_{xx}}{I_{yy}}\dot{\phi}\dot{\psi} \tag{17}$$

$$\ddot{\psi} = \frac{U_4 + \tau_{B.\psi}}{I_{zz}} + \frac{I_{xx} - I_{yy}}{I_{zz}}\dot{\phi}\dot{\theta} \tag{18}$$

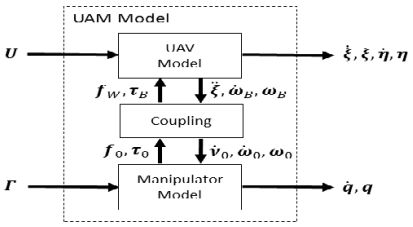

Fig. 2: Block diagram of UAM Model.

D. Forward kinematics

Introducing the following notations

- $\boldsymbol{\xi}_T = [x_T \ y_T \ z_T]^T$ is the cartesian coordinates vector of the manipulator end effector in the inertial frame,
- $\boldsymbol{\eta}_T = [\phi_T \ \theta_T \ \psi_T]^T$ is the Euler angles vector of the manipulator end effector in the inertial frame,
- $\boldsymbol{\kappa} = [\boldsymbol{\xi}_T^T \ \boldsymbol{\eta}_T^T]^T$,
- $\boldsymbol{\zeta} = [\boldsymbol{\xi}^T \ \psi \ \boldsymbol{q}^T]^T$,

the forward kinematics relating $(\dot{\boldsymbol{\zeta}}, \boldsymbol{\zeta})$ and $(\dot{\boldsymbol{\kappa}}, \boldsymbol{\kappa})$ reads as

$$\dot{\boldsymbol{\kappa}} = \boldsymbol{T}(\boldsymbol{\eta}_T)^{-1}\Big[\boldsymbol{J}_\zeta(\boldsymbol{\zeta}, \theta, \phi)\dot{\boldsymbol{\zeta}} + \boldsymbol{J}_\beta(\boldsymbol{\zeta}, \theta, \phi)[\dot{\theta} \ \dot{\phi}]^T\Big] \tag{19}$$

with $\boldsymbol{T}(\boldsymbol{\eta}_T)$ the transformation matrix defined as

$$\boldsymbol{T}(\boldsymbol{\eta_T}) = \begin{bmatrix} 0 & -S\psi_T & C\psi_T C\theta_T \\ 0 & C\psi_T & S\psi_T C\theta_T \\ 1 & 0 & -S\theta_T \end{bmatrix} \tag{20}$$

and $\boldsymbol{J}_\zeta(\boldsymbol{\zeta}, \theta, \phi)$ (respectively $\boldsymbol{J}_\beta(\boldsymbol{\zeta}, \theta, \phi)$) the Jacobian matrix for the kinematics of $\boldsymbol{\zeta}$ (respectively $[\theta \ \phi]^T$). For more details on the forward kinematics equation (19), the reader can refer to Arleo *et al* [15].

III. Control design

A full block diagram for the control of UAM system is shown in Fig. 3. It consists of a closed-loop inverse kinematics (CLIK) algorithm for the computation of the motion references and two motion controllers, the first one for quadrotor and the other one for the manipulator arm.

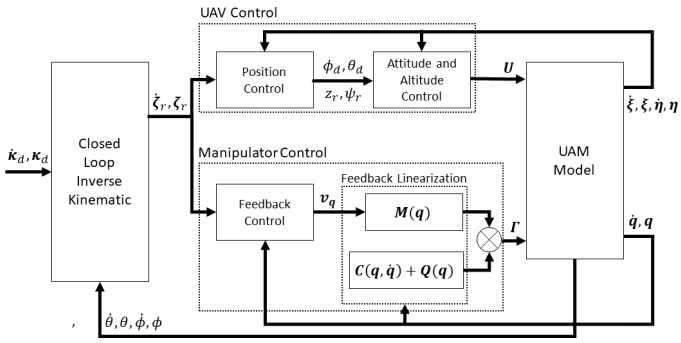

Fig. 3: Full block diagram of UAM control.

A. CLIK algorithm and reference trajectories

Recalling forward kinematics (19) and considering the CLIK [16] as shown in Fig. 4, the computation of the reference trajectories $(\dot{\boldsymbol{\zeta}}_r, \boldsymbol{\zeta}_r)$ from desired trajectory $(\dot{\boldsymbol{\kappa}}_d, \boldsymbol{\kappa}_d)$ is given by

$$\begin{aligned}\dot{\boldsymbol{\zeta}}_r = \boldsymbol{J}_\zeta^\dagger(\boldsymbol{\zeta}_r, \theta, \phi)\, \boldsymbol{T}(\boldsymbol{\eta}_{T.r})\, (\dot{\boldsymbol{\kappa}}_d + \boldsymbol{K}\boldsymbol{e}) \\ - \boldsymbol{J}_\zeta^\dagger(\boldsymbol{\zeta}_r, \theta, \phi)\, \boldsymbol{J}_\beta(\boldsymbol{\zeta}_r, \theta, \phi)\, [\dot{\theta} \ \dot{\phi}]^T\end{aligned} \tag{21}$$

where $\boldsymbol{J}_\zeta^\dagger$ is a least damped squares inverse of $\boldsymbol{J}_\zeta$ [17], $\boldsymbol{K}$ is a symmetric positive definite gain matrix and $\boldsymbol{e} = \boldsymbol{\kappa}_d - \boldsymbol{\kappa}_r$ is tracking error vector. $\boldsymbol{\kappa}_r$ is end effector position and orientation reference trajectory calculated from (19) from computed value $\boldsymbol{\zeta}_r$ and measured value $[\theta \ \phi]^T$. Here, $(\dot{\boldsymbol{\kappa}}_d + \boldsymbol{K}\boldsymbol{e})$ is a feedback gain for the compensation of tracking error due to numerical approximation of $\boldsymbol{J}_\zeta^\dagger$.

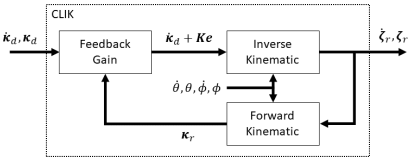

Fig. 4: Closed-loop inverse kinematic block diagram.

B. UAV Control

UAV control system is designed in hierarchical manner with inner and outer control loops as shown by Fig. 3.

1) Outer Control

Outer position control gives the roll (ϕ_d) and pitch (θ_d) angles desired trajectories derived from dynamic equation (1) and (2) as [18]

$$\begin{bmatrix}\phi_d \\ \theta_d\end{bmatrix} = \frac{m}{U_1}\begin{bmatrix}S\psi & -C\psi \\ C\psi & S\psi\end{bmatrix}\begin{bmatrix}v_\phi \\ v_\theta\end{bmatrix} \tag{22}$$

v_ϕ and v_θ allowing to control x- and y- *position* as [19]

$$v_\phi = K_{p.x}(x_d - x) + K_{i.x}\int(x_d - x) - K_{d.x}\dot{x} \tag{23}$$

$$v_\theta = K_{p.y}(y_d - y) + K_{i.y}\int(y_d - y) - K_{d.y}\dot{y} \tag{24}$$

with x_d and y_d the respective desired positions. Notice that the evaluation of (22) requires that U_1 has not to be zero: the condition will be fulfilled in the sequel given that U_1 will

control the altitude z and that, during the flight, U_1 has to compensate the gravity effect then equals mg.

2) Inner Control

To illustrate STWC design, only the UAV altitude (z) control is developed in the sequel. The other controller ($\phi, \theta, \psi, q_1, q_2$) will follow a same procedure. The design consists of two phases. Firstly is the design of sliding variable, σ_z. The most typical sliding variable is given as:

$$\sigma_z = \dot{e}_z + \lambda_z e_z, \quad \lambda_z > 0 \tag{25}$$

$$\dot{\sigma}_z = \ddot{z} - \ddot{z}_r + \lambda_z(\dot{z} - \dot{z}_r) \tag{26}$$

where $e_z = z - z_r$ is the difference between the reference altitude (z_r) and the measured altitude (z). The STWC is a second order sliding mode controller and ensures in a finite time $\sigma_z = \dot{\sigma}_z = 0$. Then, when both these objectives are reached, the system trajectories will converge to origin [20] by following these two equations.

$$\dot{e}_z = -\lambda_z e_z, \quad \ddot{e}_z = -\lambda_z \dot{e}_z \tag{27}$$

Secondly is the design of control law to force system trajectories towards the objectives described by the sliding variable in spite of the presence of perturbations and uncertainties. Consider the control U_1 defined as

$$U_1 = \frac{m(\ddot{z}_r - \lambda_z(\dot{z} - \dot{z}_r) + u_z + g)}{C\theta C\phi} \tag{28}$$

By replacing U_1 defined as (28) in (15), one gets

$$\ddot{z} = \ddot{z}_r - \lambda_z(\dot{z} - \dot{z}_r) + u_z + \frac{f_{W,z}}{m} \implies \dot{\sigma}_z = u_z + \frac{f_{W,z}}{m} \tag{29}$$

In order to get a robust closed-loop system, u_z reads as the STWC [21]

$$u_z = -K_{1.z}|\sigma_z|^{1/2}\text{sign}(\sigma_z) + v_z \tag{30}$$
$$\dot{v}_z = -K_{2.z}\text{sign}(\sigma_z)$$

The other control inputs are defined by a similar and read as

$$U_2 = I_{xx}(\ddot{\phi}_d - \lambda_\phi(\dot{\phi} - \dot{\phi}_d) + u_\phi) - (I_{yy} - I_{zz})\dot{\theta}\dot{\psi} \tag{31}$$

$$U_3 = I_{yy}(\ddot{\theta}_d - \lambda_\theta(\dot{\theta} - \dot{\theta}_d) + u_\theta) - (I_{zz} - I_{xx})\dot{\phi}\dot{\psi} \tag{32}$$

$$U_4 = I_{zz}(\ddot{\psi}_r - \lambda_\psi(\dot{\psi} - \dot{\psi}_r) + u_\psi) - (I_{xx} - I_{yy})\dot{\theta}\dot{\phi} \tag{33}$$

with u_ϕ, u_θ and u_ψ also defined as STWC.

C. Manipulator Control

For high dynamic accuracy, it is necessary to take into account manipulator dynamic model using a computed torque control technique [14] [22]. As a consequence, the control input vector $\mathbf{\Gamma}$ is defined as

$$\mathbf{\Gamma} = \boldsymbol{M(q)\nu_q} + \boldsymbol{C(q,\dot{q})\dot{q}} + \boldsymbol{Q(q)} \tag{34}$$

Computed torque manipulator control as shown in Fig. 3 consists of inner feedback linearization to compensate the non-linearities of the robot dynamics [14] and an outer loop defining the control signal $\boldsymbol{\nu_q}$. Replacing the control law (34) into the dynamical model of the manipulator (7) yields

$$\boldsymbol{\ddot{q}} = \boldsymbol{\nu_q} \tag{35}$$

As previously, a STW based control (34) is defined with

$$\boldsymbol{\nu_q} = \boldsymbol{\ddot{q}_r} - \boldsymbol{\lambda_q}(\boldsymbol{\dot{q}} - \boldsymbol{\dot{q}_r}) + \boldsymbol{u_q} \tag{36}$$

with $\boldsymbol{u_q}$ defined, for each articulation q_i ($i \in \{1, 2\}$),

$$u_{q_i} = -K_{1.q_i}|\sigma_{q_i}|^{1/2}\text{sign}(\sigma_{q_i}) + v_{q_i} \tag{37}$$
$$\dot{v}_{q_i} = -K_{2.q_i}\text{sign}(\sigma_{q_i})$$

with $\sigma_{q_i} = \dot{q}_i - \dot{q}_{r_i} + \lambda_i\,(q_i - q_{r_i})$.

D. Gain Adaptation Law

The computation of gain K_1 and K_2 requires the knowledge of the disturbance bound as discussed in Chalanga *et al* [23], Moreno *et al* [24] and Kumar [25]. This value is difficult to obtain and often leads to over-estimated values. A way to counteract this is to introduce a dynamical adaptation of the control gain that does not require any knowledge of the disturbance bound and that is sufficient to overcome the unknown uncertainties. Therefore, an adaptation law for $K_{1,*}$ and $K_{2,*}$ ($* \in \{z, \phi, \theta, \psi, q_1, q_2\}$) has been recently proposed [26]. The main advantage of this approcach with respect to previous ones is that it requires the tuning of only two parameters. The idea behind this adaptation law is simple: when the system is not accurate, it could be due to a too much low gain with respect to the uncertainties and perturbations. In opposition, when the system is accurate, it is not necessary to keep a high gain: this latter is then reduced. The adaptation reads as

$$\dot{K}_{1,*} = \begin{cases} \dfrac{\alpha_*}{\psi_* + \epsilon_*} & \text{if } |\sigma_*| > \epsilon_* \\ -K_{1,*} & \text{if } |\sigma_*| \leqslant \epsilon_* \end{cases} \tag{38}$$

$$\dot{K}_{2,*} = \begin{cases} \dfrac{\alpha_*}{2|\sigma_*|^{1/2}} & \text{if } |\sigma_*| > \epsilon_* \\ -K_{2,*} & \text{if } |\sigma_*| \leqslant \epsilon_* \end{cases} \tag{39}$$

$$\psi_* = |\dot{\sigma_*}| \tag{40}$$

where α_* and ϵ_* are some positive design parameters. $\dot{\sigma_*}$ is got from σ_* thanks to a standard filtering first order differentiator with a time constant denoted τ_*.

IV. SIMULATIONS

The validation of the control scheme has been made thanks to the simulation of the closed-loop system, with the following parameters for the UAV. Mass of UAV, rotor distance from CoM, thrust coefficient and torque coefficient are $2kg$, $0.25m$, $3\times10^{-5}Ns^2$ and $7.5\times10^{-7}Nms^2$ respectively. The inertia matrix reads as $\text{diag}([1.24, 1.24, 2.48])$. The UAV is equipped with 2-DOF revolute manipulator arm for which the link mass, the link length and tha moment of inertia about their joints are $0.1\ kg$, $0.25\ m$ and $0.0021\ kgm^2$ respectively. The simulation model is built using Matlab/Simulink software. In this paper, comparison is made between PID and adaptive STWC/PID controllers. Notice that x- and y-controllers have been remained as PID control for generating roll and pitch desired trajectories (see (22)). The following tables details the values of the control parameters in both cases.

A helical motion trajectory is used to evaluate the end effector tracking capability. This test is conducted either with or without introduction of external force on the system. This trajectory simulates all the translational and rotational motions simultaneously.

TABLE I: PID parameters

Parameter	K_p	K_i	K_d	Parameter	K_p	K_i	K_d
Pos X	7.5	6.42	2.19	Pos Y	7.5	6.42	2.19
Pos Z	26	18.4	9.18	Roll	108	272	10.4
Pitch	108	272	10.4	Yaw	30	22.8	9.86
Joint Q1	70	81.3	15.1	Joint Q2	70	81.3	15.1

TABLE II: Adaptive gain STWC parameters

Parameter	K_p	K_i	K_d	Parameter	K_p	K_i	K_d
Pos X	5	4.44	1.34	Pos Y	5	4.44	1.34

Parameter	λ	K_{10}	K_{20}	α	ϵ
Pos Z	10	0.1	0.1	110	0.1
Roll	30	0.1	0.1	52	0.01
Pitch	30	0.1	0.1	50	0.01
Yaw	10	0.1	0.1	148	0.1
Joint Q1	30	0.1	0.1	510	0.01
Joint Q2	30	0.1	0.1	1440	0.01

A. Without disturbance

Fig. 5-6-7 display the results obtained by considering that no perturbation is acting on the system. Two values are extracted from the simulations:

- the end effector position error, as the Euclidean distance between the desired and the actual position error; and
- the end effector rotation error, as the absolute value of the error angle as:

$$\theta_e = \left| arccos((tr({}^W\boldsymbol{R}_T{}^T\,{}^W\boldsymbol{R}_{dT}) - 1)/2) \right|$$

where ${}^W\boldsymbol{R}_{dT}$ and ${}^W\boldsymbol{R}_T{}^T$ are respectively the rotation matrices from desired and actual end effector angle calculated from quadrotor and manipulator output value.

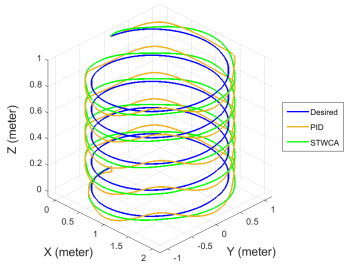

Fig. 5: 3D Trajectory of end effector.

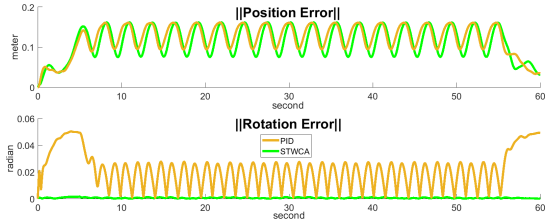

Fig. 6: End effector trajectory error versus time (sec).

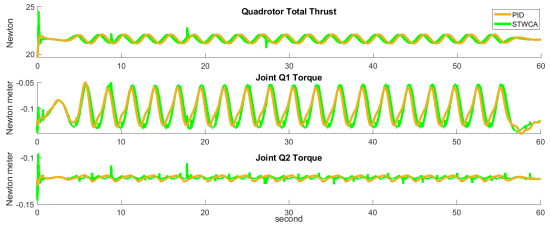

Fig. 7: End effector forces and torques versus time (sec).

Fig. 5 shows the end effector motion tracking comparison between PID (yellow), STWCA (green) with respect to the desired trajectory (blue) in the nominal case (no perturbation, no uncertainty)[1]. It shows the ability of STWCA control to force the closed-loop system trajectory close to the desired trajectory. A nominal case tracking error is shown in Fig. 6 for the two controllers (the lower the value, the better the performance). The position and rotation RMSE values of STWCA are 0.1187 and 6.8767×10^{-4} respectively as compared to PID position and rotation RMSE values of 0.1261 and 0.0246 respectively. It is clear that STWCA allows a smaller steady state error in position and rotation control. However, a significant variation of torque (with large dynamics) with STWCA (Fig. 7) could induce substantial actuator mechanical wear and tear.

B. With disturbance

1) Disturbance on UAV

The proposed control schemes are now evaluated with horizontal disturbance of 1.5N introduced along x-axis of inertial frame while UAV tracks the trajectory. Fig. 8 shows the end effector tracking error. The position and rotation RMSE value of STWCA are 0.1226 and 0.0011 respectively as compared to PID position and rotation RMSE value of 0.1279 and 0.0256 respectively. Though this horizontal disturbance affects STWCA stability, it still has better performances compared to PID.

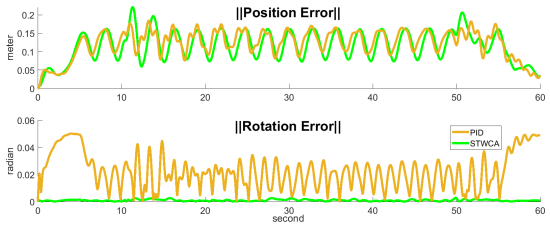

Fig. 8: End effector trajectory error with disturbance on UAV versus time (sec).

2) Disturbance on end effector

The proposed controller is now tested for mass loading by introducing a weight of 1.3N at the tip of end effector. Fig. 9 shows the tracking error of end effector with this disturbance. The position and rotation RMSE value of STWCA are 0.1187 and 7.1349×10^{-4} respectively as compared to PID position and rotation RMSE value of 0.1519 and 3.5637 respectively. It shows that with mass loading the performances of STWCA controller are less affected than those of PID controller, showing by this way its better robustness.

[1]Similar colour scheme is used for all graph.

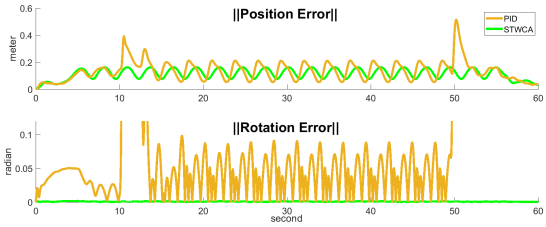

Fig. 9: End effector trajectory error with disturbance on end effector versus time (sec).

The normalized root mean square of tracking error (Fig. 10) shows that STWCA allows a better position and rotation control. Furthermore, the variation of UAV force and joint torque for STWCA is much higher than PID, that reflects a more "aggressive" actuator control to overcome the disturbance.

These simulations show that the proposed adaptive gain super twisting sliding mode control is efficient, even without the knowledge of uncertainty bound and with sufficient gain to overcome the disturbance from the arm motion and external force. It is shown that the proposed STWCA scheme is able to achieve system stability, accuracy and robustness.

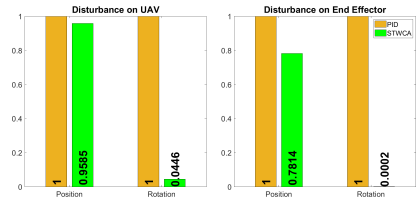

Fig. 10: End Effector normalize root mean square error.

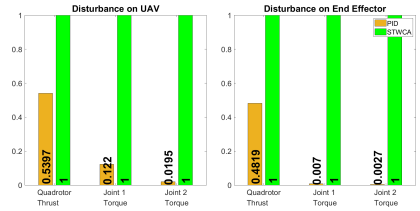

Fig. 11: End Effector normalize force and torque variation.

V. Conclusion

The paper has proposed an original PID/Adaptative super-twisting controller for the control of a UAV equipped with a manipulator arm. Thanks to simulations, the control scheme has shown its capability to control such system even with perturbation. Furthermore, the gain adaptation allows to simplify the gains tuning.

The next step is the application of this control scheme on an experimental set-up, and to evaluate very recent adaptation laws in order to further simplify the setting of the control.

References

[1] H. A. Anuar, F. Plestan, A. Chriette, and O. Kermorgant, "Sliding mode control with adaptive gain of quadrotor with rigid manipulator," in *2021 20th International Conference on Advanced Robotics (ICAR)*. IEEE, 2021, pp. 547–554.

[2] F. Ruggiero, V. Lippiello, and A. Ollero, "Aerial manipulation: A literature review," *IEEE Robotics and Automation Letters*, vol. 3, no. 3, pp. 1957–1964, 2018.

[3] N. Mimmo, A. Macchelli, R. Naldi, and L. Marconi, "Robust motion control of aerial manipulators," *Annual Reviews in Control*, vol. 49, pp. 230–238, 2020.

[4] S. Kim, S. Choi, and H. S. Kim, "Aerial manipulation using a quadrotor with a two dof robotic arm," in *2013 IEEE/RSJ International Conference on Intelligent Robots and Systems*, 2013, pp. 4990–4995.

[5] C. Zhiyuan, L. Yanyang, S. Yanhua, C. Hongyu, W. Bin, H. Mingqi, and Y. Rao, "Fuzzy sliding mode control for rotorcraft aerial manipulator with extended state observer," in *2020 Chinese Automation Congress (CAC)*. IEEE, 2020, pp. 1710–1714.

[6] Y. Chen, W. Zhan, B. He, L. Lin, Z. Miao, X. Yuan, and Y. Wang, "Robust control for unmanned aerial manipulator under disturbances," *Ieee Access*, vol. 8, pp. 129 869–129 877, 2020.

[7] C. Kuchwa-Dube and J. O. Pedro, "Altitude and attitude tracking of a quadrotor-based aerial manipulator using super twisting sliding mode control," in *Proceedings of the 6th International Conference on Control, Mechatronics and Automation*, 2018, pp. 65–69.

[8] ——, "Quadrotor-based aerial manipulator altitude and attitude tracking using adaptive super-twisting sliding mode control," in *2019 International Conference on Unmanned Aircraft Systems (ICUAS)*. IEEE, 2019, pp. 144–151.

[9] H. T. M. N. ElKholy, "Dynamic modeling and control of a quadrotor using linear and nonlinear approaches," Master's thesis, School of Sciences and Engineering, The American University in Cairo, April 2014.

[10] R. M. Murray, Z. Li, and S. S. Sastry, *A mathematical introduction to robotic manipulation*. CRC press, 2017.

[11] Y. Stergiopoulos, E. Kontouras, K. Gkountas, K. Giannousakis, and A. Tzes, "Modeling and control aspects of a uav with an attached manipulator," in *2016 24th Mediterranean Conference on Control and Automation (MED)*, June 2016, pp. 653–658.

[12] K. Gkountas, D. Chaikalis, and A. Tzes, "Force control design for a robot manipulator attached to a uav," *IFAC-PapersOnLine*, vol. 51, no. 30, pp. 548–553, 2018.

[13] W. Khalil, "Dynamic modeling of robots using recursive newton-euler techniques," in *ICINCO2010*, 2010.

[14] W. Khalil and E. Dombre, *Modeling, identification and control of robots*. Butterworth-Heinemann, 2004.

[15] G. Arleo, F. Caccavale, G. Muscio, and F. Pierri, "Control of quadrotor aerial vehicles equipped with a robotic arm," in *21St mediterranean conference on control and automation*. IEEE, 2013, pp. 1174–1180.

[16] B. Siciliano, L. Sciavicco, L. Villani, and G. Oriolo, *Robotics: modelling, planning and control*. Springer Science & Business Media, 2010.

[17] S. R. Buss, "Introduction to inverse kinematics with jacobian transpose, pseudoinverse and damped least squares methods," *IEEE Journal of Robotics and Automation*, vol. 17, no. 1-19, p. 16, 2004.

[18] D. W. Mellinger, "Trajectory generation and control for quadrotors," Ph.D. dissertation, Faculties of the University of Pennsylvania, University of Pennsylvania, Jan 2012.

[19] G. Szafranski and R. Czyba, "Different approaches of pid control uav type quadrotor," 2011.

[20] Y. Shtessel, C. Edwards, L. Fridman, and A. Levant, *Sliding mode control and observation*. Springer, 2014, vol. 10.

[21] A. Levant, "Sliding order and sliding accuracy in sliding mode control," *International journal of control*, vol. 58, no. 6, pp. 1247–1263, 1993.

[22] B. Siciliano and O. Khatib, *Springer handbook of robotics 2nd Edition*. springer, 2016.

[23] A. Chalanga and F. Plestan, "Finite time stabilization of an uncertain chain of integrators by integral sliding mode approach," *IFAC-PapersOnLine*, vol. 50, no. 1, pp. 9613–9618, 2017.

[24] J. A. Moreno, "On strict lyapunov functions for some non-homogeneous super-twisting algorithms," *Journal of the Franklin Institute*, vol. 351, no. 4, pp. 1902–1919, 2014.

[25] P. R. Kumar, A. K. Behera, and B. Bandyopadhyay, "Robust finite-time tracking of stewart platform: A super-twisting like observer-based forward kinematics solution," *IEEE Transactions on Industrial Electronics*, vol. 64, no. 5, pp. 3776–3785, 2017.

[26] M. Taleb and F. Plestan, "Adaptive supertwisting controller with reduced set of parameters," in *2021 European Control Conference (ECC)*. IEEE, 2021, pp. 2627–2632.